

***MARINE STRATUS CLOUD LIFECYCLE MODULATED BY LATENT HEAT  
FLUX IN A COASTAL OCEAN UPWELLING REGION***

Dunn, M.<sup>1</sup> and Riemer, N.<sup>2</sup>

<sup>1</sup>Environmental Sciences Department, Brookhaven National Laboratory, Upton, NY 11973-5000

<sup>2</sup>Department of Atmospheric Sciences, University of Illinois at Urbana-Champaign, Urbana, IL 61801

Submitted to  
*Journal of Geophysical Research*

September 2009

**Environmental Sciences Department/Atmospheric Sciences Division**

**Brookhaven National Laboratory**

P.O. Box 5000

Upton, NY 11973-5000

[www.bnl.gov](http://www.bnl.gov)

Notice: This manuscript has been authored by employees of Brookhaven Science Associates, LLC under Contract No. DE-AC02-98CH10886 with the U.S. Department of Energy. The publisher by accepting the manuscript for publication acknowledges that the United States Government retains a non-exclusive, paid-up, irrevocable, world-wide license to publish or reproduce the published form of this manuscript, or allow others to do so, for United States Government purposes.

This preprint is intended for publication in a journal or proceedings. Since changes may be made before publication, it may not be cited or reproduced without the author's permission.

## **DISCLAIMER**

This report was prepared as an account of work sponsored by an agency of the United States Government. Neither the United States Government nor any agency thereof, nor any of their employees, nor any of their contractors, subcontractors, or their employees, makes any warranty, express or implied, or assumes any legal liability or responsibility for the accuracy, completeness, or any third party's use or the results of such use of any information, apparatus, product, or process disclosed, or represents that its use would not infringe privately owned rights. Reference herein to any specific commercial product, process, or service by trade name, trademark, manufacturer, or otherwise, does not necessarily constitute or imply its endorsement, recommendation, or favoring by the United States Government or any agency thereof or its contractors or subcontractors. The views and opinions of authors expressed herein do not necessarily state or reflect those of the United States Government or any agency thereof.

## **Abstract**

During the summer of 2005 the Department of Energy's Atmospheric Radiation Measurement Mobile Facility (AMF) was located on the Californian coast at Point Reyes alongside a cool, oceanic, eastern boundary current and beneath a persistent marine stratus cloud deck. Mean sea surface temperatures in this region are generally low due to the coastal upwelling of cold subsurface water; however, the region also experiences some of the world's largest sea surface temperature variations. In this paper, we present extensive observations of sea surface temperatures and overlying marine stratus clouds and describe a mechanism governing the relationship between sea surface temperatures and the observed cloud lifecycle. We provide evidence for a novel hypothesis of marine stratus cloud lifecycle where the intermittent relaxation of coastal upwelling generates a large positive difference between sea surface temperature and air temperature, which, through enhanced evaporation, facilitates the delivery of water vapor aloft and initializes boundary layer stability. If hygroscopic cloud condensation nuclei are plentiful, condensation occurs, cloud liquid water path increases, and latent heat is transferred to the thickening cloud. If cloud condensation nuclei are depleted, boundary layer moisture increases, shutting down the latent heat flux. When the latent heat flux out competes cloud top cooling, the boundary layer deepens and moisture again becomes critical to cloud development. We present observations of these effects in this cool ocean region, discuss their implications for mesoscale convective structures and emphasize the importance of short temporal scale processes in global climate models.

## 1 Introduction

Marine stratus clouds persist above the eastern boundary current regions of the world's oceans and have been shown to have a significant cooling effect on the earth's climate [Hartmann *et al.*, 1992]. Despite their known importance in the climate system, marine stratus and stratocumulus remain poorly simulated even in coupled ocean-atmosphere global climate models [Karlsson *et al.*, 2007; Bony and Dufresne 2005]. The clouds, usually focused near the coast, over the eastern edge of the eastern boundary currents, extend out into the ocean in massive sheets. They are restricted in vertical development and remain close to the ocean surface due to the presence of a near-permanent capping thermal inversion [Neiburger *et al.*, 1961]. In an effort to collect information on, and better simulate these clouds, the Atmospheric Radiation Measurement Mobile Facility (AMF) was deployed at the Point Reyes National Seashore (38.1°N, 122.95°W) on the California coast during the summer of 2005.

Eastern boundary currents are driven by strong northwesterly winds that blow parallel to the coast. Near California, the winds are associated with the North Pacific High, a sub-tropical high pressure system located off the coast [Hickey 1979]. The winds strengthen during summer as increased equatorial heating serves to strengthen the high pressure feature by enhancing Hadley circulation [Huyer 1983, Strub *et al.* 1987]. Whenever the North Pacific High is energized, the associated northwesterly winds increase in magnitude.

The winds interact with the coast, along the eastern edge of the eastern boundary currents of all the world's major oceans resulting in the coastal upwelling of cool sub-surface sea waters. This occurs as the strong alongshore winds drive a large Ekman transport of warmed surface waters away from the coast [Huyer, 1983]. As the surface waters move offshore, they are replenished from below by the upwelling of colder, deeper ocean water. The stronger the winds the more water brought to the surface. Occasionally, the winds driving this upwelling will slacken or reverse direction, causing an interruption or relaxation of the upwelling phenomena [Beardsley, 1987]. This reversal driven by either a weakened North Pacific High pressure system or a synoptic disturbance, allows warm surface waters to flow offshore instead of cold [Send *et al.*, 1987].

Although upwelling areas comprise a small portion of the eastern boundary region they can have a profound impact on the ocean surface water temperatures by delivering cold sub-surface water and warmed inshore waters for as many as 300 km out to sea [Brink and Cowles, 1991]. Sea surface temperature (SST) changes have been known to affect some of the physical characteristics of stratus and stratocumulus (stratiform) clouds [e.g. Klein *et al.*, 1995; Bretherton

and Wyant 1997; Pincus *et al.*, 1997] however, our understanding of the influence SST on the presence and persistence of the overlying stratiform clouds has been lacking. For instance, in a recent investigation into the effects of varying SST's on stratiform cloud amount over the cool waters of the equatorial Pacific cold tongue, [Mansbach and Norris 2007] find anomalies in monthly cloud amount and SST advection are strongly correlated however, the output from global climate models fail to simulate the observed cloud–SST advection relationship. As is typical of SST-cloud interaction studies, they question why nearby regions, with the same climatology remain cloud free.

By combining measurements gathered at the coastal AMF site with those from an offshore NOAA buoy, this paper presents a unique set of observations of an increase in SSTs resulting from a relaxation of coastal upwelling directly influencing the physical properties and the development of coastal marine stratiform clouds. We hypothesize that the relative difference between SST and the overlying air temperature (AT) modulates the flux of water vapor, hence latent heat, to the boundary layer and that the condensation of water vapor on atmospheric aerosols during cloud formation releases latent heat which contributes to the stability commonly associated with marine stratus development. First, we will present the observed relationships between SST and cloud liquid water path and then the statistical correlations between those two variables and the concentration of atmospheric aerosols. Next, a single upwelling-relaxation cycle is presented in detail. Finally, we use variations in atmospheric stability to identify the conditions necessary for marine stratus cloud development and lifecycle.

## **2 Data and Methodology**

The AMF was deployed on the California coast at Point Reyes (38.1°N, 122.95°W ) from April 2 through September 14, 2005 as part of the Marine Stratus Radiation, Aerosol, and Drizzle (MASRAD) Intensive Operation period [Miller *et al.*, 2005]. This coastal site, located 1.2 km from the ocean is an ideal place to study marine cloud lifecycle due to the persistence of low stratus and stratocumulus clouds during the summer months. The AMF consists of a suite of surface-based remote sensing instruments that take continuous observations of the cloud, aerosol, atmospheric state and radiation. Cloud liquid water path (LWP) is the vertically integrated cloud water content and must be measured with considerable accuracy in order to quantify cloud/sea surface/aerosol interactions. To accomplish this, data from the 2-channel (23.8 and 31.4 GHz) microwave radiometer is processed through a set of physical and statistical retrieval algorithms (MWRRET) which serves to reduce a LWP bias and improve LWP retrievals [Turner *et al.*

2007]. A water collection problem on the instrument window occurred sporadically from April 2 through June 24 therefore, data from that time period were omitted from the analysis.

In addition to the microwave radiometer, a zenith pointing narrow beam ( $0.24^\circ$ ) 94 GHz Doppler cloud radar operated by the University of Miami, collected high temporal (2 second) vertical velocity profiles and cloud boundaries over the site. Vertical profiles consisted of 35 spatially resolved height bins of 30 m range gates, ranging in altitude from 75 m to 1095 m. The instrument operated at the lower limit of its spatial capabilities due to the generally low altitude of marine stratus clouds, which resulted in considerable system interference in the lower bins. Signal quality was improved by applying a variance/non-calibrated power filtering scheme to remove interference. In-cloud velocities that exhibited coherent signals were included in the analysis. The filtered, high signal-to-noise ratio data were examined for drizzle events through the use of a drizzle mask, derived from anomalies in the first and second moments of the radar spectra [Kollias and Albrecht, 2000]. Reflectivity could not be calibrated due to high levels of interference; however, relative reflectivity returns from the radar are used to determine cloud top height estimates. A collocated laser ceilometer operating at near infrared wavelength (905 nm) measured cloud base height to within about 5 m.

In addition, radiosondes were released four times daily at 6-hour intervals, over the course of the deployment and provided information on the vertical profiles of temperature, humidity, pressure, horizontal wind speed and direction. The height of the local inversion base was determined from the radiosonde-derived vertical temperature profile and identified as the altitude where the temperature begins to increase with height.

Potential cloud condensation nuclei (CCN) were measured at a height of 10 m using a Continuous-Flow Streamwise Thermal Gradient Cloud Condensation Nuclei Counter [Roberts and Nenes, 2005]. The instrument brings ambient aerosols into a sample chamber and alters the internal supersaturation through a predetermined set of seven supersaturation (SS) set points (0.18, 0.29, 0.44, 0.58, 0.85, 1.12 and 1.37). Hygroscopic aerosols or condensation nuclei (CN) are activated to become CCN. The number of CCN measured at a supersaturation was determined every minute with five measurements at each of the seven SS set points. The CCN data set from July 01, 2005 to September 15, 2005 was used to create a smoothed, linearly interpolated, time series at each SS set point. The seven complete time series were used to construct a saturation spectrum at one-minute intervals. The full seven-point individual spectra were fitted to a logarithmic curve and the number of CCN at 1% SS determined for every time point.

Sea Surface temperatures were measured at a National Oceanic and Atmospheric Administration (NOAA) National Water Level Observation network buoy (World Meteorological

Organization station number 9415020), located at 38.00° N 122.98° W, approximately 11 km from the land based AMF site. In order to confirm that buoy SST measurements are in fact associated with the coastal upwelling process, an upwelling index [*Bakun*, 1973] for the region was employed. Real-time assessments of the Upwelling Index (UI) are calculated by the Environmental Research Division of the NOAA Fisheries Service. They are derived through estimates of the geostrophic wind stress calculated from 6-hourly means of 3° global pressure fields and made available through the Pacific Fisheries Environmental Laboratory Website at <http://www.pfeg.noaa.gov/products/PFEL/modeled/indices/upwelling/NA/>.

### **3 Cloud liquid water path and sea surface temperature: Observations during MASRAD**

Marine boundary layer clouds observed during the field campaign have a thickness mean ( $\mu$ ) of 193 m, a standard deviation ( $\sigma$ ) of 59 m and contain an average of 78 g m<sup>-2</sup> ( $\sigma = 62$  g m<sup>-2</sup>) of liquid water in a vertical path. Cloud thickness is measured as the difference in altitude between the ceilometer measured cloud base and the radar-measured cloud top. LWP information is gained by applying an algorithm to the data collected by the microwave radiometer. The clouds oscillate between two forms: a thin, low liquid water path stratus form and a thick, high liquid water path (>100 g m<sup>-2</sup>) stratocumulus form. Figure 1 gives an overview of how LWP relates to cloud thickness, and demonstrates a linear relationship. This indicates that an increase in LWP is primarily due to cloud thickening. Drizzle is known to increase with increasing cloud thickness [*Nichols*, 1987]. This is confirmed by our data as radar-derived in-cloud drizzle markers, a function of drop fall velocity and backscattered power, indicate an increase in the occurrence of drizzle in thick clouds relative to thin clouds.

The AMF site located at Point Reyes, California, exists in a region of strong contrasts. In addition to the oscillation between thick and thin clouds there exists an oscillation in SST just offshore. The dramatic fluctuations in SST are due to the coastal upwelling of cold subsurface water [*Brink and Cowles*, 1991]. These SST changes commonly occur in summer and result from strong northwesterly winds, which blow parallel to the California coast moving sea surface waters along with them. The surface waters are also influenced by the Coriolis force, which, in the northern hemisphere, acts to transport the surface water to the right of the wind through Ekman transport. As cool surface waters move offshore, they are replenished from below by the upwelling of colder, deep ocean water. The strength and direction of the winds, as well as the

local topography, factor into the intensity and frequency of upwelling [Pringle and Dever 2009]. The stronger the winds, the greater the volume of cold water brought up.

At Point Reyes the alongshore winds are driven by large-scale forcing. A pressure gradient forms between the North Pacific High located in the middle of the Pacific Ocean around 40°N 140°W [Winant *et al.*, 1988] and a strong low pressure feature found over land. Occasionally, the winds driving the upwelling will slacken or reverse direction, causing an interruption or relaxation of the upwelling phenomena. The two images in Figure 2 are weekly nighttime composites of clear-sky satellite views, which provide a glimpse of SST features during each of these conditions. These composite images were created by removing pixels that contained clouds and interpolating through them. In Figure 2a cold water is present along the coast and offshore waters are generally cool (10 to 15 °C). In contrast, very warm waters (14 to 18°C) are associated with a recent (July 17-20) relaxation of upwelling as shown in Figure 2b.

Figure 3 shows the time series for SST and LWP over the three-month period from June 22 to September 15. SSTs were measured every hour at the National Water Level Observation network buoy just offshore of the AMF site, and data downloaded from the NOAA National Data Buoy Center <http://www.ndbc.noaa.gov/> web site. In order to confirm that buoy SST measurements we gathered were in fact associated with the coastal upwelling process, an Upwelling Index (Bakun, 1973) for the region is employed. Real-time assessments of the Upwelling Index (UI) are calculated by the Environmental Research Division of the NOAA Fisheries Service. A high index number is indicative of fierce alongshore winds and strong upwelling. A low index number indicates extremely weakened or absent upwelling conditions. In Figure 3a buoy measured SST is shown to negatively correlate with coastal upwelling in the region. The strong correlation (correlation coefficient of -0.532) between this index and SSTs measured at the buoy just offshore of Point Reyes lends confidence to the fact that the SST measurements reflect upwelling conditions.

The cyclic nature of upwelling in this area is evident by the roughly 7-day period exhibited in the time series of the upwelling Index and is also reflected in the SSTs. In Figure 3b, the same SST time series is depicted along with one-minute measurements of cloud LWP whenever LWP is greater than 100 g m<sup>-2</sup>. Low LWP measurements less than 100 g m<sup>-2</sup> are eliminated from this figure for visual clarity and will be explained later. The high-LWP, thick clouds appear correlated with the increases in SST. One single event of a relaxation of upwelling resulting in higher SSTs and thickened, high LWP clouds is labeled as Event #3 in both Figures 3a and 3b and will be discussed later in this text. The overall increasing trend in SST seen in these figures reflects the seasonal changes that occur as the summer progresses. From these two figures

it is evident that a correlation exists between SSTs modulated by coastal upwelling and cloud development just offshore of the Point Reyes AMF site.

To investigate this relationship in more detail, hourly SST measurements and the nearest corresponding cloud LWP measurement, were binned according to 1°C-temperature-intervals. Only nighttime values were included in this analysis (local time between 2200 and 0500 hours, from July 1 to September 15). Daytime values were eliminated due to the effects of solar radiative heating on LWP measurements. For each temperature bin, the maximum recorded LWP is reported. The resulting relationship is shown in Figure 4.

Figure 4 demonstrates the robust relationship that exists between SST and the maximum measured cloud LWP. LWP values in this figure are binned which eliminates effects of subadiabaticity such as diurnal variability. The relationship is non-linear if the SST full range from 9.2°C to 15.6°C is considered. LWP increases with increasing SST up to 13.3°C, beyond this threshold it decreases. This seems contrary to the findings of *Norris and Leovy* [1994] who reported a negative correlation between surface observations of seasonal mean marine stratiform cloud amount and SST. This negative correlation is a widely accepted finding. However, their investigation and most subsequent, assess SST on a longer, usually monthly, time scale and fail to capture the short term effects of the upwelling-relaxation relationships.

To explain our finding we postulate the following hypothesis, which we will then substantiate in the remainder of this section: The positive correlation between cloud LWP and SST in this generally cool upwelling region is based on an increase in the delivery of water vapor from the sea surface to the cloud. The increased water vapor aloft is the result of an increase in latent heat flux from the ocean to the atmosphere. It is the relative, instantaneous temperature difference between the ocean and atmosphere that drives the flux in this inversion-capped boundary layer. This simple relationship applies up to a certain SST threshold. At that point the MBL tends to become saturated, sea surface evaporation ceases and the latent heat flux is turned off. Boundary layer saturation is achieved when condensation aloft is constrained.

### **3.1 Relationship between SST and inversion height**

The inversion height plays an important role in the relationship of SST and LWP. It can be controlled by any one of a number of processes depending on the atmospheric conditions. When the inversion height is very low, it limits the cloud thickness and hence LWP, as these two quantities are directly related (compare Figure 1). Generally, the boundary layer becomes deeper as the temperature of the ocean beneath warms [*Emanuel*, 1994] and surface warming of the

MBL out-competes radiative cooling. An increase in the height of the inversion with increasing SST has been widely reported [Wyant and Bretherton, 1997; Stevens, 2007]. In most cases, the rise in inversion base is generally attributed to enhanced cloud top entrainment. The enhanced entrainment then serves to reduce the inversion strength, which leads to a continued drying of the MBL and cloud dissipation.

In our observations, the varying altitude of the inversion base reflects changes in SST as shown in Figure 5a. Low SSTs, less than about  $11.5^{\circ}\text{C}$ , are associated with a mean inversion height of only 280 m. Comparing with Figure 1, this corresponds to a LWP of less than about  $100\text{ g m}^{-2}$ . However, as SST increases above  $13.3^{\circ}\text{C}$ , the inversion base rises with maximum values of 800 m. This is when high liquid water clouds with  $\text{LWP} > 100\text{ g m}^{-2}$  occur, as marked by the diamonds in Figure 5a. On an ocean basin scale, a low inversion is found over generally cool waters then rises as the water beneath warms. Bretherton and Wyant [1997] modeled this effect, referred to as the deepening-warming hypothesis and attribute inversion rise to increased surface winds and turbulence structures found over warm waters. This explanation could not apply to the observations in Figure 5a, as boundary layer winds are observed to slightly decrease in magnitude ( $\mu=3.5$ ,  $\sigma=1.2\text{ m sec}^{-1}$ ) during the warm water/relaxation phase ( $\text{UI}<125$ ) and increase ( $\mu=4.1\text{ m sec}^{-1}$ ,  $\sigma=1.6$ ) during the cool phase of upwelling. This non-linear relationship depicted in this figure is consistent with the SST-LWP relationship shown in Figure 4. The maximum in LWP and inversion height occurs for a certain SST, in our case about  $13.3^{\circ}\text{C}$ . As SST rises further, additional water vapor is delivered to the boundary layer, as will be shown in the next section. When the inversion height increases, the inversion base temperature decreases; at the same time continued delivery of water vapor will increase the buoyancy and warm the boundary layer. This process continues until a point where the inversion breaks down and enhanced cloud top entrainment causes drying of the BL and cloud dissipation. This is the life cycle of the marine stratiform clouds. It is important to note that both of these parameters, SST and inversion height, are ultimately driven by the same large-scale atmospheric feature, the North Pacific High.

### 3.2 Relationship between SST and latent heat flux

Changes in the observed SSTs are reflected in the difference between the SST and the temperature of the air just above it. Figure 5b demonstrates this relationship and shows that thick, high LWP clouds are abundant when the SST is warmer than the boundary layer air; a scenario that occurs exclusively at SSTs greater than  $11.5^{\circ}\text{C}$ . Surface air temperatures remain fairly

constant throughout the study period with a mean reading at 13.1°C ( $\sigma = 1.8^\circ\text{C}$ ), therefore as SSTs increase the magnitude of the SST-AT difference becomes larger.

Due in part to these observations, we suspect that the transfer of latent heat from the sea surface to the atmosphere plays an important role in explaining the relationship between SST and LWP. We therefore estimated latent heat fluxes with the bulk transfer equations described by *Gill* [1982]:

$$Q_L = \rho_a L_E C_L U_{10} (q_s - q_a), \quad (1)$$

where  $\rho_a = 1.3 \text{ kg m}^{-3}$  is the density of air,  $L_E = 2.501 \cdot 10^6 \text{ J kg}^{-1}$  is the latent heat of evaporation and  $C_L = 1.35 \cdot 10^{-3}$  the latent heat transfer, Stanton coefficient. The variable  $U_{10}$  is wind speed at 10 m above the surface. The specific humidity at the sea surface and near the surface at 10 m height in the atmosphere is  $q_s$  and  $q_a$ , respectively. Specific humidity in the atmosphere ( $q_a$ ) is calculated from instantaneous radiosonde measurements of surface dew point, temperature and pressure collected 10 m AGL every six hours at the coastal AMF site. Calculations of specific humidity at the sea surface ( $q_s$ ) assume the relative humidity near the ocean surface is 100% and the skin temperature right at the sea surface is the same as the SST, which are obtained from six-hour averages of buoy measurements. Note that saturation vapor pressure was not corrected for the effects of salinity, which would reduce the values by a negligible amount. It is known that the latent heat transfer coefficient is sensitive to atmospheric stability [*Oost et al.*, 1999]. The coefficient employed here is for stable conditions, which our analysis in Section 6, below shows is appropriate.

Although the AMF site is within 5.7 miles of the offshore buoy, the use of ground based wind measurements as proxy for ocean-collected data in the heat flux calculations should be questioned. An attempt was made to validate this approach by examining the association between the along-shore velocity component of the wind and the buoy measured wave height, which should be positively correlated. A robust correlation  $R^2=0.98$  was found between the buoy-collected wave height measurements ( $\mu = 2.2\text{m}$ ,  $\sigma = 0.6$ ) and the north-south component of the ground based wind velocity during upwelling. Also, the World Meteorological Organizations standard definition for surface air measurements is 10 m AGL this corresponds to 24 m ASL at the AMF ground site. The ground measurements for  $T_a$ ,  $U_{10}$  and  $q_a$  used in Equation 1 could be extrapolated to 10 m ASL; however, we accept the small errors that accompany this uncertainty. In fact, the overall resulting latent heat flux values did not change appreciably even when wind speed was set to a constant, mean value of  $3.8 \text{ m sec}^{-1}$  ( $\sigma = 1.4$ ).

Figure 5c shows the relationship of latent heat flux, according to equation (1) and SST. The latent heat flux is positive when a large amount of moisture is delivered from the ocean to the atmosphere. This occurs when SST is greater than AT. In an earlier investigation into the relationships between SST and latent heat flux, *Zhang and McPhaden* [1995] found that with cool SST, latent heat increases with increasing SST and with warm SST it decreases with increasing SST. They point out that the difference between the humidity of the overlying air and the saturation humidity at the sea surface interface drives the latent heat increase. These results gathered over the equatorial Pacific Ocean agree with the findings here even though they examined SST changes without taking into account the overlying air temperature. We find the air sea temperature differences crucial to understanding the flux of latent heat under varying SST conditions. Throughout our study, during upwelling and relaxation times, air temperature ( $\mu = 13.1^\circ\text{C}$ ,  $\sigma = 1.8^\circ\text{C}$ ) does not vary by much more than  $2^\circ\text{C}$ .

Grey diamonds in Figure 5c indicate high LWP clouds and are predominately found with a positive heat flux. The few high LWP values with a negative flux are likely the result of a lag time required for cloud dissipation. The radiosonde measurements are captured once every 6 hours however, SST and LWP are collected on time-scales of 1 hour or 1 minute and then averaged around the radiosonde time by 6 hours or 5 minutes respectively. There are instances where despite a positive latent heat flux the cloud remained a low LWP cloud ( $< 100 \text{ g m}^{-2}$ ). As shown in Figure 5a, the low LWP clouds are associated with a low capping inversion which limits vertical development. Only when the buoyant forces associated with warm surface waters are strong enough to overcome the subsidence inversion can these clouds fully develop. In these instances, it is likely that the inversion strength is enhanced although this was not measured. Low LWP clouds commonly persist during periods of cold SST and negative latent heat flux. Although the heat flux is reversed and heat is lost from the sea surface, moisture will continue to diffuse, albeit at a much slower rate, through passive diffusion [*Liu et al.*, 1979]. Molecular diffusion occurs regardless of the SST-AT temperature. These low LWP clouds probably rely on passive molecular diffusion at the sea surface as a source of water vapor. Under these conditions, it takes longer to saturate the BL and the inversion remains low due to weak buoyant forces. In addition, substantially more turbulence would be required to create the supersaturation necessary for the initiation of condensation of water vapor on aerosols.

It is important to note that at Point Reyes surface air measurements taken over land are used as a proxy for those over the water. It is likely that the land temperature readings are actually slightly warmer than those over the water, thus positively biased in our calculations. If a positive bias exists it would only serve to increase the SST-AT difference and enhance our flux

determinations. *Liu et al.* [1979] points out that assessing the effects from these small air–sea temperature differences require extremely accurate measurements. *Webster et al.* [1996] during the TOGA-COARE experiment in the tropics estimates that the 1°C error, common in global satellite SST measurements, has the potential to alter flux determinations by as much as 18 W m<sup>-2</sup>. In this coastal upwelling region with an unusually large temperature range, surface measurements can be successfully employed.

#### **4 The correlation between SST, LWP and CCN**

After having established the relationship between SST and LWP, we investigated the potential for fluctuating levels of atmospheric aerosols to modulate this effect. The availability of cloud condensation nuclei (CCN) will certainly affect the condensation of water vapor in the atmosphere and could alter the SST-LWP relationship. First, we investigate the relationship between CCN and LWP and then the statistical relationship between all three variables, SST, LWP and CCN.

It is known that cloud LWP is readily depleted through drizzle in marine stratus clouds [*Stevens et al.* 2003; *Bretherton et al.*, 2003, *Rasinski and Pawlowska*, 2006]. Drizzle also depletes CCN. *Ackerman* [1993] identifies a close coupling between CCN concentrations and marine stratus cloud lifecycles and finds that a depletion of CCN can lead to cloud dissipation. The mechanism operates through the scavenging of CCN particles in the atmosphere by falling drizzle drops. Figure 6 presents both daily averaged (dark solid line) and 1-minute (light solid line) surface based measurements of ambient CCN concentrations at 1% supersaturation in the atmosphere beneath the cloud from July 1 to September 15 at Point Reyes. Radar derived, drizzle indicators (plus signs) appear and persist as CCN concentrations are depleted. This observed correlation suggests that drizzle scavenging is operating here.

The daily predictions of the regional Upwelling Index (dotted line), which is high during the coastal upwelling of cold water, is also depicted in Figure 6. It is important to point out that as the winds driving upwelling switch direction, they are likely to deliver aerosols with varying chemical composition and activation regimes however, the chemical composition of aerosols at the AMF site appears unrelated to the CCN nucleating capacity and cloud development. In a detailed examination of the properties of MBL aerosols collected during a concurrent fields program, the MASE (Marine Stratus Experiment), at Point Reyes, CA, *Wang et al.* [2007]

concludes that the size distribution, not the chemical composition of the aerosols at Point Reyes is responsible for modulation of the CCN spectrum.

Statistical analysis of cloud LWP compared with SST reveals a positive correlation between the occurrence of thick, high LWP clouds and locally higher SSTs (correlation coefficient of 0.47) as was displayed in Figure 3b. This correlation value excludes the confounding signals of diurnal variability by including only nighttime collected data. In a preliminary evaluation of the affects of aerosols on the LWP-SST relationship the parameter C, the concentration of CCN at 1% supersaturation, is used as a proxy for the in-cloud nucleation behavior of atmospheric aerosols. A value of C less than  $500 \text{ cm}^{-3}$  is considered a low aerosol condition [Rogers and Yau 1989] and is associated with a weak nighttime C-LWP correlation coefficient of 0.18, or a negative, daytime C-LWP correlation coefficient of -0.15. Conversely, a high ambient aerosol load ( $\text{CCN} > 500 \text{ cm}^{-3}$ ) enhances the nighttime C-LWP relationship as seen in the increased correlation coefficient of 0.48. Due to the complex nature of these relationships the series is further analyzed using multivariate techniques.

The temporal relationships between LWP, SST and the atmospheric C parameter are examined through empirical orthogonal function (EOF) analysis of the nighttime collected data. EOF analysis characterizes the covariability in the time series of the variables (LWP, SST, C). Excluding diurnal signals, these three variables are observed to fluctuate on a temporal scale of 3-7 days. EOF analysis reveals that the first mode accounts for nearly all (86.2 percent) of the variability in the data. In this mode LWP and SST are positively correlated and vary together, while both are negatively correlated with C. Correlation coefficients of the first mode to the original observed data are 0.77, 0.61 and 0.68 respectively and indicate the contribution of each variable. The second mode, which explains a small portion of the variability (13.8 percent), is predominately driven by the seasonal trend in SST. Correlation coefficients of this second SST-driven mode to the observations are 0.25, 0.74 and 0.16 respectively. When the seasonal trend in SST is removed, the second mode reflects the strength of early upwelling, another SST feature.

Further investigation into the differences between the observations and the first mode reveals that at times when the LWP observations are much less than would be predicted by the mode amplitude, the C parameter is also unusually low. Figure 7 displays this feature through normalized values of C and the maximum deviation, in 0.25 unit bins, between the normalized observations of cloud LWP and the LWP amount predicted by the first mode of the principal component analysis at that time. The effects of drizzle scavenging are already incorporated into the analysis because the first mode contains the feature of a decreased C with increasing LWP. The comparison of maximum LWP modal differences to normalized CCN concentrations

depicted in Figure 7 yields a robust correlation ( $R^2 = 0.8465$ ), suggesting low CCN concentration may inhibit cloud LWP development. In a global assessment of changes in LWP with varying aerosol concentrations, *Han et al.* [2002] examined aerosol concentrations using satellite measurements of cloud droplet number concentrations (CDNC) and LWP. LWP was found to increase, decrease or stay constant with an increasing CDNC depending on the region examined. In maritime regions, a positive relationship was found, where a decrease in CDNC correlates with a decrease in LWP. Although these results are similar to those presented here, we consider the CDNC a pivot point in a balance between water vapor and available aerosols. In a marine location water vapor is generally abundant and aerosols limiting; in this situation LWP can only increase by the carrying capacity of the CCN, setting up a positive relationship.

## 5 Case study of an upwelling-relaxation cycle

A case of one upwelling-relaxation cycle from July 16 to 22 is examined in detail in Figure 8. This case study demonstrates the interplay of the different key player, i.e. SST, LWP, CCN, inversion height, that we discussed in the previous sections. The cycle is driven by winds with negative meridional velocities (from the north) occurring during upwelling. In Figure 8a, upwelling winds cease and relaxation begins on July 16. For this to occur, the driving force, the North Pacific High must weaken or shift position. Relaxation persists until the upwelling winds return again on July 22. SST begins to increase (Figure 8b) as meridional winds shift from northerly to southerly and Ekman transport of cold water from beneath the ocean surface is shut off (July 16). As the SST increases the height of the subsidence inversion also rises (dashed line in Figure 8e), however, this is still a relatively shallow boundary layer. This inversion rise is demonstrated previously in Figure 5a. When SST is at a maximum the inversion has elevated and may be weakened so much that it no longer caps convection. Corresponding to the increase in SST and inversion base height is an increase in the cloud LWP (Figure 8d). Diurnal variations in LWP are pronounced as clouds form during the evening and dissipate as solar radiation warms the lower atmosphere. High LWP clouds occur as the SST reaches about 13 degrees and persist for a period of four days (July 18 to 22) during the relaxation phase. LWP is increased by cloud thickening, a result a slight descent of cloud base at night and a gradual rise of cloud top (grey line in Figure 8e). Cloud base height, measured by ceilometer (Figure 8e), exhibits a strong diurnal signal (data not shown). In general, cloud base rises to greater than 200 m at about 10am local time and continues to be high until about 7 pm. It is lowest, usually less than 100 m, at night from about 2am to 7am with a minimum height at about 4am. Cloud base will reach a maximum

altitude in the afternoon around 1pm. From August 15 on through the study period, clouds that form in the morning persist throughout the day.

Frequently after clouds thicken, drizzle occurs. Figure 8c contains drizzle markers at times when the radar signal indicated (described earlier) the presence of falling drizzle droplets. Drizzle continues until the clouds return to a thin state on July 22. In this figure, drizzle appears to gradually deplete CCN concentrations, probably through drizzle scavenging. In all of the seven upwelling-relaxation events observed, a decline in CCN concentration correlates with an increased frequency of drizzle as previously demonstrated in Figure 6. In this way, as described by *Ackerman et al.* [1993], clouds act to limit their own lifetime. For example, from July 19 to 22, drizzle predominates and 93.4% of CCN were removed from the potential condensation nuclei (CN) measured in the marine boundary layer during this time. We do not know the exact supersaturation experienced by the aerosols so we use the  $C$  parameter (ambient CCN concentration at 1% supersaturation) again to represent their behavior.  $C$  increases steadily up to the point of drizzle occurrence and then the concentration begins to decrease. When CCN concentrations are very low ( $C$  less than  $500 \text{ cm}^{-3}$ ) but SST temperatures and inversion height are at a maximum, as occurred on July 22, the cloud does not reach high LWP status. This case exemplifies our previous statements.

As is evident in Figure 8, cloud dissipation is a key component of the marine stratus cloud lifecycle. We propose a mechanism of cloud dissipation where the drizzle-scavenging of CCN leads to a decrease in condensation aloft, which then allows for the accumulation of water vapor in the boundary layer beneath the capping inversion. When SST-AT is positive, sensible and latent heat is delivered to the atmosphere; the BL expands and weakens the inversion base enough to enhance entrainment mixing across it. A deeper, drier BL further enhances ocean evaporation and promotes latent heat flux by increasing the humidity difference across the air-sea interface. In the air, the transport of water vapor relies on turbulent motions; however at the sea surface interface, molecular diffusion operates and is a much slower, rate-limiting process (*Liu et al.* 1979). Evidence of this may be seen in Figure 9 where relative humidity in the lower atmosphere increases logarithmically with increasing cloud LWP. In this figure relative humidity is binned by 5% and maximum LWP value in that bin is reported. The lower atmosphere is defined here as the height at one-tenth of the total BL depth and corresponds roughly to the 1000 hPa level. Evaporation at the sea surface cannot continue when the BL air is saturated with respect to water vapor, which occurs if condensation aloft ceases. Condensation will cease as CCN are depleted. The decrease in condensation aloft creates a highly unstable condition. Drizzle collecting on the sea surface could also retard the transfer of latent and sensible heat to the

boundary layer; however drizzle is usually light in this region and ocean mixing vigorous. The high LWP clouds persist during high relative humidity as long as condensation continues.

## 6 Stability

It has long been known that an empirical relationship exists between marine stratus cloud cover and atmospheric stability [*Slingo*, 1980; *Klein and Hartman* 1993; *Wood and Bretherton* 2006]. Atmospheric stability is assessed by vertical gradients in potential temperature. *Klein and Hartman* [1993] found that atmospheric stability, which they define as the difference between potential temperatures measured at the sea surface and that of the 700-hPa level, is highly correlated with low marine stratus cloud cover. Globally, regions of cold monthly mean SST were found to have greater stability. It is known that in cold upwelling regions stability is maintained by an “upside down convection” where radiative cooling and dry air entrainment at the cloud top creates dense sinking air. [*Karlsson et al.*, 2008]. Also, *Rosenfeld et al.* [2006] suggests that enhanced stability is caused by cooling beneath the cloud through the evaporation of drizzle.

For this study we examine the relationship of LWP and atmospheric stability not on a climatological time scale but on shorter (6 hour) time scales. As a measure of stability we define the vertical difference in potential temperature ( $\Delta\theta$ ) from the lower one-tenth BL to the upper tenth BL  $\theta(0.9 z_i) - \theta(0.1 z_i)$ , where  $z_i$  is the inversion height. The lower tenth of the MBL generally represents a well-mixed state of the lower atmosphere. Figure 10a shows the relationship of LWP and  $\Delta\theta$  for all data points collected from July 1 to Sept 1, 2005. Based on this figure we segregate the data into three regimes: (1) Negative  $\Delta\theta$ , associated with thin, low LWP clouds; (2) Positive  $\Delta\theta$ , following a linear trend of increasing cloud LWP with increasing stability. We consider this regime as more typical of marine stratus clouds and in agreement with previous studies [*Klein and Hartman* 1993, *Wood and Bretherton* 2006]. These points are marked with black dots. (3) Finally, contained within the box drawn in Figure 10a are “anomalous” points where this LWP/stability relationship does not hold true and large  $\Delta\theta$  is associated with low LWP clouds. From this figure it is also easy to see why data collected from low LWP clouds, which commonly occur, can confound strict relationships with other environmental variables.

To understand the separation into these three regimes in more detail we map the data points from the three regimes in a way that relates vertical differences (Upper-Lower) in atmospheric conditions to the corresponding  $\Delta\theta$ . Displayed in Figure 10b the differences in equivalent potential temperatures,  $\Delta\theta_e$  are compared with  $\Delta\theta$ . For moist-adiabatic processes  $\theta_e$  is a conserved quantity, so in this case  $\Delta\theta_e$  is zero. We see that this applies for the points from regime

(2), which cluster around the line for  $\Delta\theta_e=0$ . This means that the increase in  $\theta$  with height, a positive  $\Delta\theta$ , observed in Figure 10a is due to latent heat release when condensation occurs. The points related to regimes (1) and (3), both corresponding to low LWP clouds, display negative and positive  $\Delta\theta_e$ , respectively. To explain this we consult the relationship of  $\Delta\theta$  to two other quantities, the difference in water vapor mixing ratio,  $\Delta r$ , versus  $\Delta\theta$ , and the difference in air temperature taken from the inversion base to the low atmosphere,  $\Delta T_{air}$  versus  $\Delta\theta$ . First  $\Delta r$  is examined in Figure 10c. For points in group (2) applies that high LWP is coinciding with negative  $\Delta r$ , i.e.  $r_{upper} < r_{lower}$ . From this observation we conclude that positive  $\Delta\theta$  is maintained by removing atmospheric water vapor aloft and not through the evaporation of drizzle as is commonly thought. This reasoning also explains the dependency of  $\Delta\theta$  on  $\Delta\theta_e$ : As condensation occurs, latent heat is released in the upper atmosphere thus increasing  $\Delta\theta$ . The fact that we have included both day and night time measurements, collected during both non-drizzle and drizzling occurrences, reinforces our skepticism of precipitation as the driving mechanism. Hence, we suggest an alternative explanation, namely latent heating driven by condensation of atmospheric water vapor on aerosols in the upper boundary layer creates the stability commonly associated with marine stratiform clouds. As for points in group (3) we see that  $\Delta r$  is positive, i.e.  $r_{upper} > r_{lower}$ . This feature is unique to group (3) and segregates the two types of low LWP clouds. It appears that in this case condensation of water vapor is not occurring aloft. In addition, the high  $\Delta\theta_e$  values seen in Figure 12b reflect the additional water vapor contained in the upper BL at these times. Figure 10d reveals the cause of the apparent lack of condensation aloft observed for group (3). In this figure, the vertical difference in dry air temperature ( $\Delta T_{air}$ ) measured from the bottom of the boundary layer to the inversion base is plotted against  $\Delta\theta$ . The inversion base temperature represents the dry temperature of the air, at an altitude where the atmospheric temperature begins to dramatically increase with height. The anomalous data points from regime (3) segregate in the lower right portion of the plot at a positive  $\Delta T_{air}$  indicating that, for these cases, the dry temperature at the inversion base is higher than at the surface. For these conditions we expect vertical motions to be suppressed, hence high LPW clouds cannot develop. Although these points vary considerably in time, they have some commonalities. In addition to the positive  $\Delta T_{air}$ , the meteorological conditions prevalent when they occurs include an abrupt change in wind direction resulting in a southward wind, blowing recently upwelled cold waters beneath a low (<300m height) inversion.

In a marine environment, the environmental lapse rate should lie between the dry adiabatic lapse rate of approximately  $-9.8$  °C/km, for unsaturated air and the nonlinear moist adiabatic lapse rate (typically about  $-6.5$  °C/km) for saturated air. Our calculated  $\Delta T_{air}$  varies

between 1 and -7 °C for an inversion altitude of between 100 and 900 m. With the exception of data points from regime (3), most of the cloud cases in this study show  $\Delta T_{air} < 0$ . For data points from regime (2)  $\Delta T_{air}$  converts into an environmental lapse rate of 6.1 °C/km ( $\sigma = 1.0$  °C/km), right at the moist adiabat, when the varying height of the inversion base is taken into account. In this very shallow marine boundary layer with a mean thickness of 351 m, a change in lapse rate of 2.1 °C, which might arise through a rise or descent of the inversion base height, could determine the difference between cloud formation and dissipation.

In summary we come to the following conclusion regarding the three regimes: Both regimes (1) and (3) are not favorable for the development of high LWP clouds, but for different reasons. Regime (1) is characterized by a negative  $\Delta r$  as shown in Figure 10c, a low  $\Delta \theta_e$  as shown in Figure 12b, and a large  $\Delta T_{air}$  (negative lapse rate) as shown in Figure 12d. Therefore LWP remains low. Regime (3) is characterized by a positive  $\Delta r$ , a very high  $\Delta \theta_e$  but a positive lapse rate. LPW of clouds, which had to have formed prior to the development of this condition, remains low as well. Only for regime (2) where a negative  $\Delta r$ , zero or slight positive  $\Delta \theta_e$  and a negative lapse rate applies, high LWP clouds can develop, and then a positive  $\Delta \theta$  is created as a result of latent heat release when condensation occurs.

The difference between the SST and the air temperature (AT) in the lower boundary layer is a crucial parameter linked to the development of atmospheric stability. In this region, SST-AT can vary as both a positive or negative value with a maximum difference of about 3°C. The overall relationship between SST-AT and stability is seen in Figure 11. The high LWP points, marked with diamonds, fall above the zero SST-AT difference or when the SST is relatively warmer than the atmosphere. In contrast, a considerably warmer atmosphere in relation to the underlying cool SST is linked with low stability. These changes in SST yield dramatic changes in marine stratus clouds.

## 7 Conclusions

We have presented a case study where the lifecycle of mid-latitude marine stratus clouds is modulated by changes in the underlying SST. We show that increasing SSTs raise the SST-AT temperature difference and subsequently deliver an exponentially increasing amount of atmospheric water vapor, hence latent heat, to the developing clouds. We find as much as 22.3  $W m^{-2}$  changes in latent heat flux resulting from a 1°C change in SST, similar to that reported by *Webster et al.* [1996] (18  $W m^{-2}$ ), during the TOGA COARE experiment in the tropics. Using

coastal data collected at the DOE ARM Mobile Facility located on the California coast at Point Reyes, we took advantage of the large SST variability that occurs along the eastern edge of eastern boundary currents where coastal upwelling occurs to study this effect. We discover that although mean SSTs are usually low in upwelling regions, it is in fact the relaxation of the upwelling process, the intermittent presence of warmer coastal waters, which drives the development of stratocumulus over the eastern boundary of the North Pacific. This small-scale variability is often overlooked when climate models incorporate temporally averaged SST data.

Large SST-AT differences alone are not sufficient for marine stratiform clouds to develop. They do, however, provide one of the necessary components, water vapor. The increased warming from the sea surface is shown to raise the inversion base to a height above the LCL. We speculate that this occurs as sensible and latent heating from below out-competes radiative cloud top cooling. We have provided evidence for our hypothesis that above the LCL, the overabundance water vapor can follow one of two paths: condense on atmospheric aerosols and form a cloud, or if hygroscopic CCN are not readily available, remain in the BL, thus increasing the relative humidity. In this way a delicate balance occurs between water vapor and available CCN. Over land CCN are plentiful and water vapor is generally limiting, but over the ocean, where water vapor is sporadically plentiful, CCN are a limiting factor to cloud development. Through EOF analysis we present evidence to support our “balance hypothesis” whereby predicted cloud LWP is shown to be altered by low CCN concentrations. In a general form this balance should appear region specific, for instance in this highly polluted environment we find few instances of very low aerosol concentrations. Over the ocean, where potential CCN are not readily replenished, this imbalance should be more evident.

We show evidence of a cloud dissipation mechanism whereby saturation of the BL inhibits evaporation at the sea surface and shuts off the flux of latent heat to the BL. We have evidence that a paucity of atmospheric aerosols contributes to BL saturation. We have corroborated previous findings of the ACE2 and DYCOMS-II experiments [*Rasinski and Pawlowska, 2006*] where a positive relationship exists between the amount of liquid contained within a cloud and the propensity of those clouds to drizzle. We observe the removal of atmospheric aerosols, which we have demonstrated possess the potential to form cloud condensation nuclei (CCN), from the boundary layer through the drizzle scavenging process.

Finally, we have demonstrated that stable conditions in the lower troposphere, known to be empirically associated with marine stratus cloud amount, are predominately the result of the latent heat flux. The rate at which latent heat is delivered to the MBL controls the degree of

atmospheric stability. In this way, stability in the lower atmosphere is a consequence of cloud development, not a prerequisite.

Limited in their vertical extent by a persistent inversion, marine stratiform clouds develop across the ocean surface. We propose that the mechanism just described may also serve to modify the stratus deck after it has formed. Increases in SST, arising from warm mesoscale eddies, facilitate the sporadic delivery of excess water vapor and initiate drizzle. In an assessment of mesoscale cellular convective (MCC) forms in marine stratus clouds over the global oceans, *Agee et al.* [1973] showed that closed MCC forms preferentially over cold ocean currents and open MCC forms preferentially over warm ocean currents. Open MCC is usually associated with a higher inversion and increased drizzle [*Wood et al.* 2008]. *Petters et al.* [2006] also points out that a scarcity of CCN maintains the open MCC cells however, the mechanism is unknown. *Wood and Hartman* [2006] and *Rosenfeld et al.* [2006] hypothesized that the missing mechanism is internal to the BL and involves the impacts of aerosols on cloud microstructure, precipitation and vertical energy fluxes. We suggest that the mechanism we have just proposed, whereby warm surface currents facilitate the delivery moisture to the stratus deck, forcing drizzle scavenging and forming open pockets of MCC, provides a plausible mechanism. The similarities between this upwelling study and marine stratus MCC cloud formations warrants further investigation of an interdisciplinary nature.

This view of marine stratus cloud lifecycle focuses on a balance between atmospheric water vapor and available atmospheric aerosols, where the role of precipitation is mainly to modulate aerosol levels. The well-known indirect radiative effects, which significantly alter the ability of marine stratus clouds to reflect solar radiation and influence global temperatures, easily integrate into this perspective. The *Albrecht* [1989] indirect aerosol effect operates as the relative number of CCN increases along with increasing moisture. Such as scenario would occur if a plume were to be injected into a moistening atmosphere. The *Twomey* [1980] effect is only apparent when cloud LWP is held constant; then adding more aerosols, but not liquid, would decrease cloud droplet effective radius. Both the first and second aerosol indirect effects, (*Twomey and Albrecht*) operate within this scheme.

We present a novel mechanism for a marine stratus cloud lifecycle and suggest that it be incorporated into climate models to more accurately simulate future climate change. Predicted changes in the large-scale pressure fields resulting from global climate change could affect the strength and timing of upwelling-relaxation cycles. Recent investigations [*LaDochy, 2007; Bakun 1990*] indicate that the present trends towards increased upwelling, attributed to greater temperature contrasts between the land and sea (higher heat capacity of seawater relative to land)

should continue. A global warming of SST coupled with stronger meridional winds would serve to increase the amount of stratocumulus as long as industrial pollution continues to increase. This increase in stratocumulus amount can act as a negative feedback due to radiative effects. Large-scale, temporal air-sea interactions such as the PDO or ENSO events could also serve to modify these effects. We have presented a simple yet elegant explanation for marine stratus cloud lifecycle. This is yet another way in which water vapor, the strongest greenhouse gas known, could amplify or mitigate changes in the global climate.

### **Acknowledgements**

This work was supported by the U.S. Department of Energy, Office of Biological and Environmental Research, Climate and Environmental Sciences Divisions Atmospheric Radiation Measurement Program. Data is downloaded from the program archive ([www.archive.arm.gov](http://www.archive.arm.gov)). The SST data set was downloaded from the National Oceanic and Atmospheric (NOAA) National Data Buoy Center <http://www.ndbc.noaa.gov/> web site. Upwelling Index (UI) calculated by the Environmental Research Division of the NOAA Fisheries Service are available from the Pacific Fisheries Environmental Laboratory Website at <http://www.pfel.noaa.gov/products/PFEL/modeled/indices/upwelling/NA/>.

Special thanks to Pavlos Kollias and Mark Miller. Additional thanks to Dave Turner for his help with the microwave radiometer LWP product, John Ogren and Elisabeth Andrews for their help with CCN data.

## References

- Ackerman, A. S., O. B. Toon, and P. V. Hobbs (1993), Dissipation of marine stratiform cloud and collapse of the marine boundary layer due to the depletion of cloud condensation nuclei by clouds, *Science*, 262, 226–229.
- Agee, E. M., T. S. Chen, and K. E. Dowell (1973), A review of mesoscale cellular convection, *Bull. Am. Meteorol. Soc.*, 54, 1004–1012. [\[CrossRef\]](#)
- Albrecht, B.A. (1989), Aerosols, Cloud Microphysics, and Fractional Cloudiness, *Science*, 245 (4923), 1227 - 1230.
- Bakun, A., (1973), Coastal upwelling indices, west coast of North America, 1946-71, *U.S. Dept. of Commerce, NOAA Tech. Rep.*, NMFS SSRF-671.
- Bakun, A. (1990), Global climate change and intensification of coastal ocean upwelling, *Science*, 247, 198-201.
- Beardsley, R.C., L.K. Rosenfeld, C. E. Dorman, C. A. Friehe and C. D. Winant (1987), Local atmospheric forcing during the Coastal Ocean Dynamics Experiment1. a description of the marine boundary layer and atmospheric conditions over a northern California upwelling region, *J. Geophys. Res.*, 92, 1467-1488.
- Bony, S., and J.-L. Dufresne (2005), Marine boundary layer clouds at the heart of tropical cloud feedback uncertainties in climate models, *Geophys. Res. Lett.* 32, L20806, doi:10.1029/2005GL023851.
- Bretherton, C.S., and M.C. Wyant (1997), Moisture Transport, Lower-Tropospheric Stability, and Decoupling of Cloud-Topped Boundary Layers, *J. Atmos. Sci.*, 54, 148–167.
- Bretherton, C.S., T. Uttal, C.W. Fairall, S.E. Yuter, R.A. Weller, D. Baumgardner, K. Comstock, R. Wood, and G.B. Raga (2004), The Epic 2001 Stratocumulus Study, *Bull. Amer. Meteor. Soc.*, 85, 967–977.
- Brink K. H. (1983), The near-surface dynamics of coastal upwelling, *Prog Oceanogr*, 12, 223–257.
- Brink, K. H., and T. J. Cowles (1991), The coastal transition zone program, *J. Geophys. Res.*, 96(C8), 14,637–14,647. [\[AGU\]](#)
- Emanuel, K. A. (1994), Atmospheric convection, Oxford University Press (New York), pp. 580 ISBN: 0-19-506630-8
- Gill, A.E. (1982), Atmosphere-ocean dynamics. *International Geophysics Series 30*. London: Academic Press. pp663.
- Han, Q., W. B. Rossow, J. Zeng, and R. Welch (2002), Three different behaviors of liquid water path of water clouds in aerosol-cloud interactions. *J. Atmos. Sci.* 59, 726–733.

- Hartmann, D. L., M. E. Ockert-Bell, and M. L. Michelson (1992), The effect of cloud type on Earth's energy balance: Global analysis, *J. Climate*, 5, 1587-1606.
- Hickey, B.M. (1979), The California Current System-hypotheses and facts, *Progress in Oceanography*, 8, 191-279.
- Huyer, A.(1983), Coastal Upwelling in the California Current System, *Prog.Oceanog.*, 12, .259-284.
- Karlsson, Johannes; Svensson, Gunilla; Rodhe, Henning (2008), Cloud radiative forcing of subtropical low level clouds in global models, *Climate Dynamics*, 30, No 7-8, 779-788.
- Karlsson, J., G. Svensson, J. Teixeira, and S. Cardoso (2008), The transition from stratus topped to trade-wind cumulus topped marine boundary layer in global climate models, *18th Symposium on Boundary Layers and Turbulence, Stockholm, Sweden*.  
[http://ams.confex.com/ams/18BLT/techprogram/paper\\_139994.htm](http://ams.confex.com/ams/18BLT/techprogram/paper_139994.htm)
- Klein, S. A., and D. L. Hartmann (1993), The seasonal cycle of low stratiform clouds, *J. Clim.*, 6, 1588-1606.[CrossRef]
- Klein, S. A., D. L. Hartmann and J. R. Norris (1995), On the relationships among low cloud structure, sea surface temperature and atmospheric circulation in the summertime northeast Pacific, *J. Clim.*, 8, 1140-1155.
- Kollias, P. and B. A. Albrecht (2000), The turbulence structure in a continental stratocumulus cloud from millimeter-wavelength radar observations, *J. Atmos. Sci.*, 57, 2417-2434.
- LaDochy S., P. Ramirez and W. C. Patzert (2007), Southern California upwelling: Is recent weakening a result of global warming? *19th Conference on Climate Variability and Change San Antonio, TX*. 2007. <http://ams.confex.com/ams/pdfpapers/119047.pdf>.
- Liu, W. T., Katsaros, K. B. and J. S. Businger (1979), Bulk Parameterization of Air-Sea Exchanges of Heat and Water Vapor Including the Molecular Constraints at the Interface, *J. Atmos. Sci.* 36, 1722-1735.
- Mansbach, D. K., and J. R. Norris (2007), Low-level cloud variability over the equatorial cold tongue in observations and GCMs, *J. Climate*, 20, 1555-1570.
- Miller, M. A., A. Bucholtz, B. A. Albrecht, and P. Kollias, 2005: Marine Stratus Radiation, Aerosol, and Drizzle (MASRAD) science plan. [Online]. Available: <http://www.arm.gov/publications/programdocs/doe-er-arm-0501.pdf>
- Neiburger, M., D. S. Johnson, and C. Chien (1961), Studies of the structure of the atmosphere over the eastern Pacific Ocean in Summer, I, The inversion over the eastern North Pacific Ocean. *Univ. Calif. Publ. Meteor.*, 1, 1-94.
- Nicholls, S. (1987), A model of drizzle growth in warm, turbulent, stratiform clouds, *Q. J. R. Meteorol. Soc.*, 113, 1141-1170.

Norris, J. R., and C. B. Leovy (1994), Interannual variability in stratiform cloudiness and sea surface temperature, *J. Climate*, 7, 1915-1925.

Oost, W.A., C.M.J. Jacobs and C. Van Oort (2000), Stability Effects on Heat and Moisture Fluxes at Sea, *Boundary-Layer Meteorology*, 95 (2), 271-302. 10.1023/A:1002678429212.

Petters, M. D., Snider J. R., Stevens, B., Vali, G., Faloon, I., and L. Russell (2006), Accumulation mode aerosol, pockets of open cells, and particle nucleation in the remote subtropical Pacific marine boundary layer, *J. Geophys. Res.*, 111, D02206, doi:10.1029/2004JD005694,

Pincus, R., M. B. Baker and C. S. Bretherton (1997), What Controls Stratocumulus Radiative Properties? Lagrangian Observations of Cloud Evolution, *J. Atmos. Sci.*, 54, 2215-2236.

Pringle, J. M., and E. P. Dever (2009), Dynamics of wind-driven upwelling and relaxation between Monterey Bay and Point Arena: Local-, regional-, and gyre-scale controls, *J. Geophys. Res.*, 114, C07003, doi:10.1029/2008JC005016.

Rasinski, P., H. Pawlowska and W. W. Grabowski (2006), Drizzle formation in marine stratocumulus cloud – experimental and modeling studies. Presented at The 12th Conference on Atmospheric Radiation/12th Conference on Cloud Physics, 10-14 July 2006, Madison, WI.

Roberts, G., and A. Nenes (2005), A Continuous-Flow Streamwise Thermal-Gradient CCN Chamber for Atmospheric Measurements, *Aerosol. Sci. Technol.*, 39, 206–221.  
Rogers, R. R., and M. K. Yau (1989), *A short course in cloud physics*, 293 pp., Elsevier Science Press

Rosenfeld, D., Kaufman, Y. J., and I. Koren (2006), Switching cloud cover and dynamical regimes from open to closed Benard cells in response to the suppression of precipitation by aerosols, *Atmospheric Chemistry & Physics Discussions*, 6, 1179 -1198.

Send, U., R. C. Beardsley, and C. D. Winant (1987), Relaxation from upwelling in the coastal ocean dynamics experiment, *J. Geophys. Res.*, 92, 1683–1698. [\[AGU\]](#)

Slingo, J. M. (1980), A cloud parameterization scheme derived from GATE data for use with a numerical model, *Quart. J.R. Met. Soc.*, 106: 747–770

Stevens, B., D.H. Lenschow, G. Vali, H. Gerber, A. Bandy, B. Blomquist, J.L. Brenguier, C.S. Bretherton, F. Burnet, T. Campos, S. Chai, I. Faloon, D. Friesen, S. Haimov, K. Laursen, D.K. Lilly, S.M. Loehrer, S.P. Malinowski, B. Morley, M.D. Petters, D.C. Rogers, L. Russell, V. Savic-Jovicic, J.R. Snider, D. Straub, M.J. Szumowski, H. Takagi, D.C. Thornton, M. Tschudi, C. Twohy, M. Wetzel, and M.C. van Zanten (2003), Dynamics and Chemistry of Marine Stratocumulus—DYCOMS-II, *Bull. Amer. Meteor. Soc.*, 84, 579–593.

Stevens, B. (2007) On the Growth of Layers of Non-precipitating Cumulus Convection, *J. Atmos. Sci.*, 64, 2916-2931.

- Strub, P., J. Allen, A. Huyer, R. Smith, and R. Beardsley (1987), Seasonal cycles of currents, temperatures, winds, and sea level over the northeast Pacific continental shelf: 35°N to 48°N, *J. Geophys. Res.*, *92*, 1507–1526. [\[AGU\]](#)
- Turner, D. D., S. A. Clough, J. C. Liljegren, E. E. Clothiaux, K. Cady-Pereira and K. L. Gaustad, 2007: Retrieving liquid water path and precipitable water vapor from Atmospheric Radiation Measurement (ARM) microwave radiometers, *IEEE Trans. Geosci. Remote Sens.*, *45*, 3680–3690, doi:10.1109/TGRS.2007.903703.
- Twomey, S. (1980), Cloud nucleation in the atmosphere and the influence of nucleus concentration levels in atmospheric physics, *J. Phys. Chem.*, *94*, 1459–1463.
- Wang, J., Y.-N. Lee, P. H. Daum, J. Jayne, and M. L. Alexander (2008), Effects of aerosol organics on cloud condensation nucleus (CCN) concentration and first indirect aerosol effect, *Atmos. Chem. Phys.*, *8*, 6325–6339.
- Webster, P. J., C. A. Clayson, and J. A. Curry (1996), Clouds, radiation, and the diurnal cycle of sea surface temperature in the tropical western Pacific, *J. Climate*, *9*, 1712–1730.
- Winant, C., R. Beardsley, and R. Davis (1987), Moored wind, temperature, and current observations made during coastal ocean dynamics experiments 1 and 2 over the northern California continental shelf and upper slope, *J. Geophys. Res.*, *92*, 1569–1604. [\[AGU\]](#)
- Winant, C., C. Dorman, C. Friehe, and R. Beardsley (1988), The Marine Layer off Northern California: An Example of Supercritical Channel Flow, *J. Atmos. Sci.*, *45*, 3588–3605.
- Wood, R., and C. S. Bretherton (2006), On the Relationship between Stratiform Low Cloud Cover and Lower-Tropospheric Stability, *J. Climate*, *19*, 6425–6432.
- Wood, R., and D. L. Hartmann (2006), Spatial variability of liquid water path in marine low cloud: The importance of mesoscale cellular convection, *J. Clim.*, *19*, 1748–1764.
- Wood, R., K. K. Comstock, C. S. Bretherton, C. Cornish, J. Tomlinson, D. R. Collins, and C. Fairall (2008), Open cellular structure in marine stratocumulus sheets, *J. Geophys. Res.*, *113*, D12207, doi:10.1029/2007JD009371
- Wyant, M. C., C. S. Bretherton, H. A. Rand, and D.E. Stevens (1997), Numerical simulations and a conceptual model of the stratocumulus to trade cumulus transition, *J. Atmos. Sci.*, *54*, 168–192.
- Zhang, G.J., and M.J. McPhaden, (1995), The relationship between sea surface temperature and latent heat flux in the Equatorial Pacific, *J. Climate*, *8*, 589–605.

## Figures

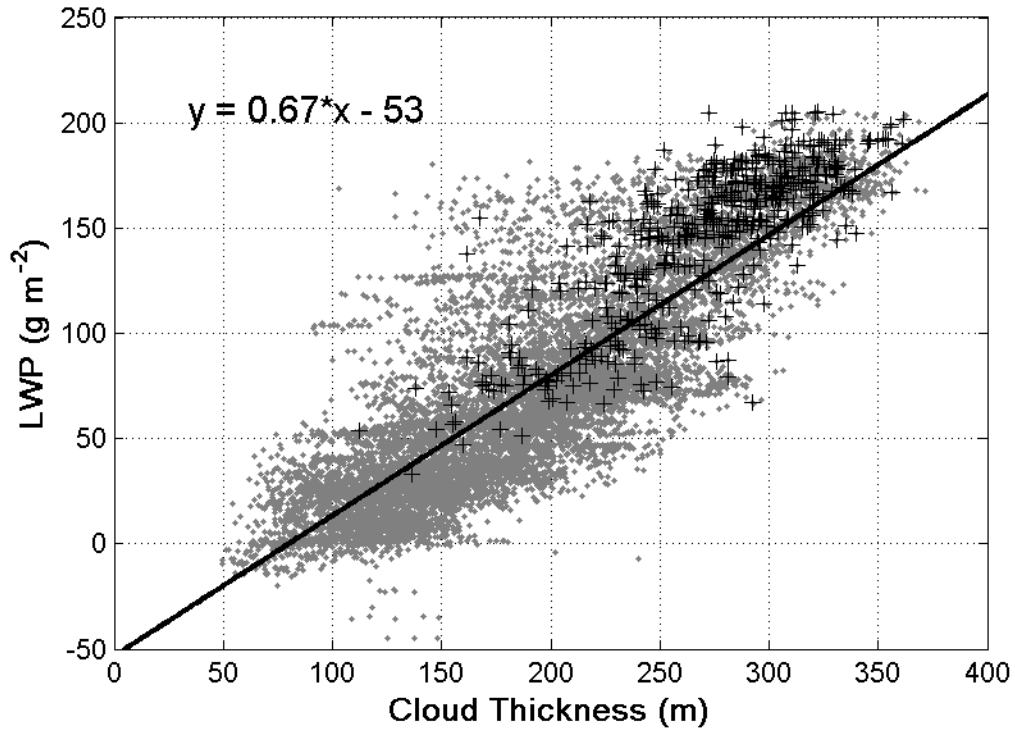
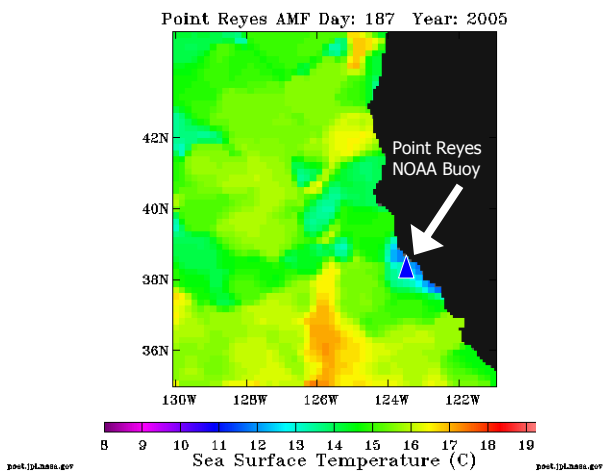


Fig. 1: One minute averages of cloud thickness, calculated as the difference between ceilometer determined cloud base and radar determined cloud top (dots) and MWR measured Liquid water path with radar derived one minute drizzle markers (cross) included. Data collected from July 1 to Sept 15, 2005.

## Upwelling



## Relaxation

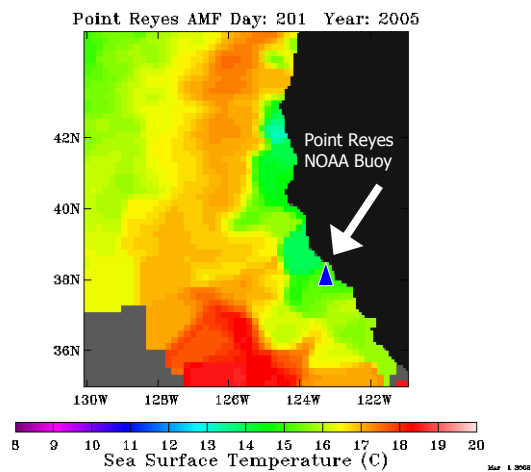
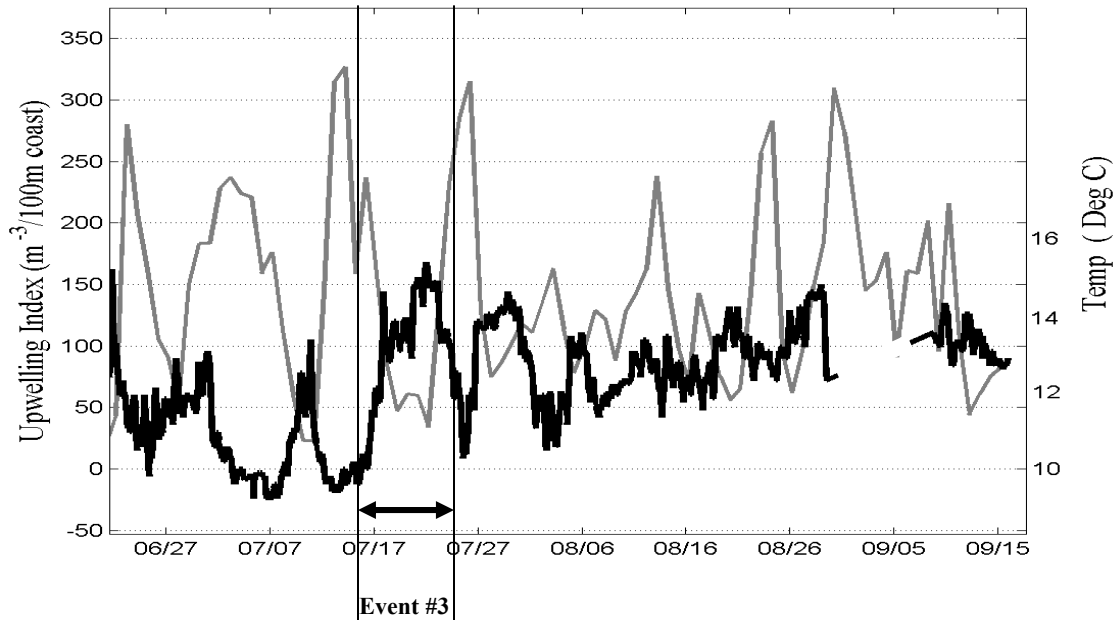


Fig. 2: NAVOCEANO MC-SST weekly nighttime SST maps with clouds removed. Week of July 6 during an upwelling event (left). Week of July 20 nearing the end of a relaxation of upwelling (right). Images are derived from the NOAA (National Oceanic and Atmospheric Administration)-Polar Orbiting Advanced Very High Resolution Radiometer (AVHRR) and obtained through the online PO.DAAC Ocean ESIP Tool (POET) at the Physical Oceanography Distributed Active Archive Center (PO.DAAC), NASA Jet Propulsion Laboratory, Pasadena, CA. <http://podaac.jpl.nasa.gov/poet>. Offshore NOAA operated buoy is marked with a triangle.

a.



b.

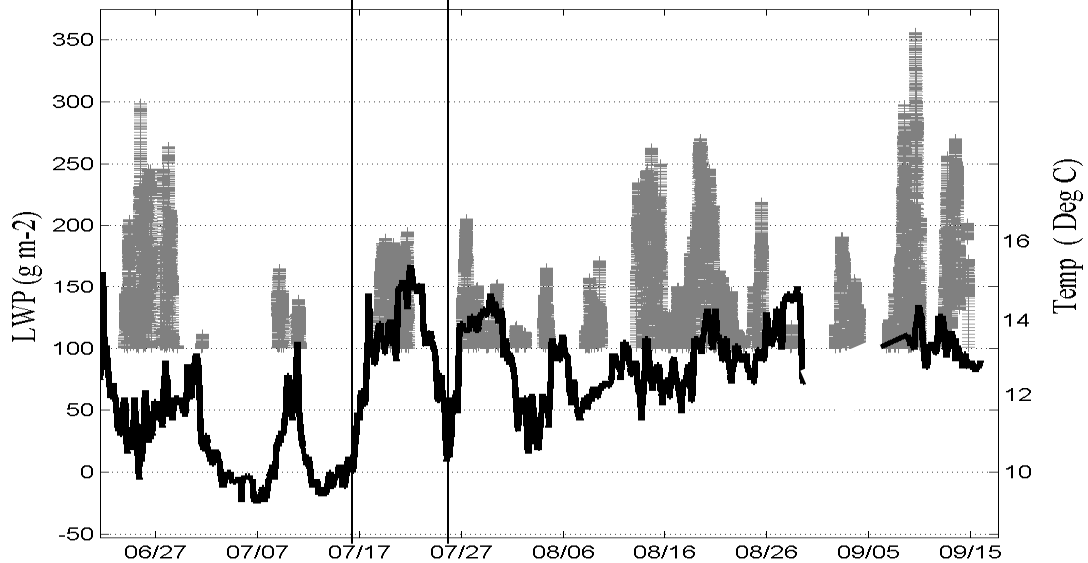


Fig. 3: Time series of Upwelling Index, SST and LWP. a.) A daily coastal upwelling index (grey line) and buoy hourly measured sea surface temperature. Upwelling index units in units of m<sup>-3</sup> of water per 100 m of coastline are calculated by NOAA Fisheries Service, Environmental Research Division. Double arrow and vertical lines indicate intensive study period of Event #3. b.) Offshore NOAA Buoy hourly measured sea surface temperature (black line) and the 1 minute occurrence of liquid water path with value greater than 100g m<sup>-2</sup> (grey +). Data collected June 22-Sept. 15, 2005, except SST missing Aug 28-Sept 8.

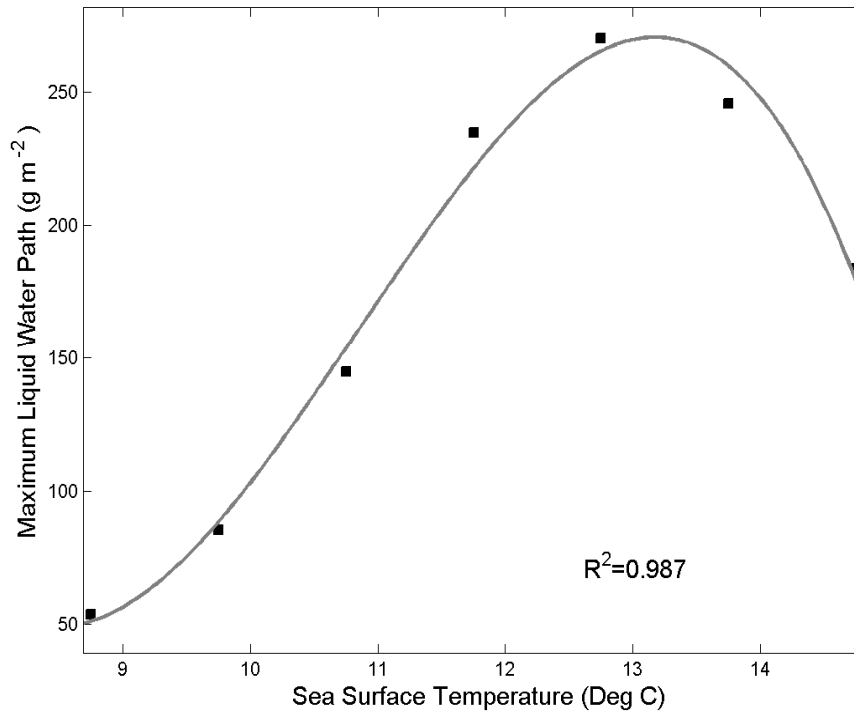


Fig. 4: Hourly nighttime observations of sea surface temperatures binned to 1°C intervals and the maximum value of the corresponding LWP observations in each temperature bin. Nighttime is defined as local time between 2200 and 0500 hrs. Data from hourly observations collected from July 1 to Sept 15, (except 8/29 to 9/08 when SST data was not available); n=1113.

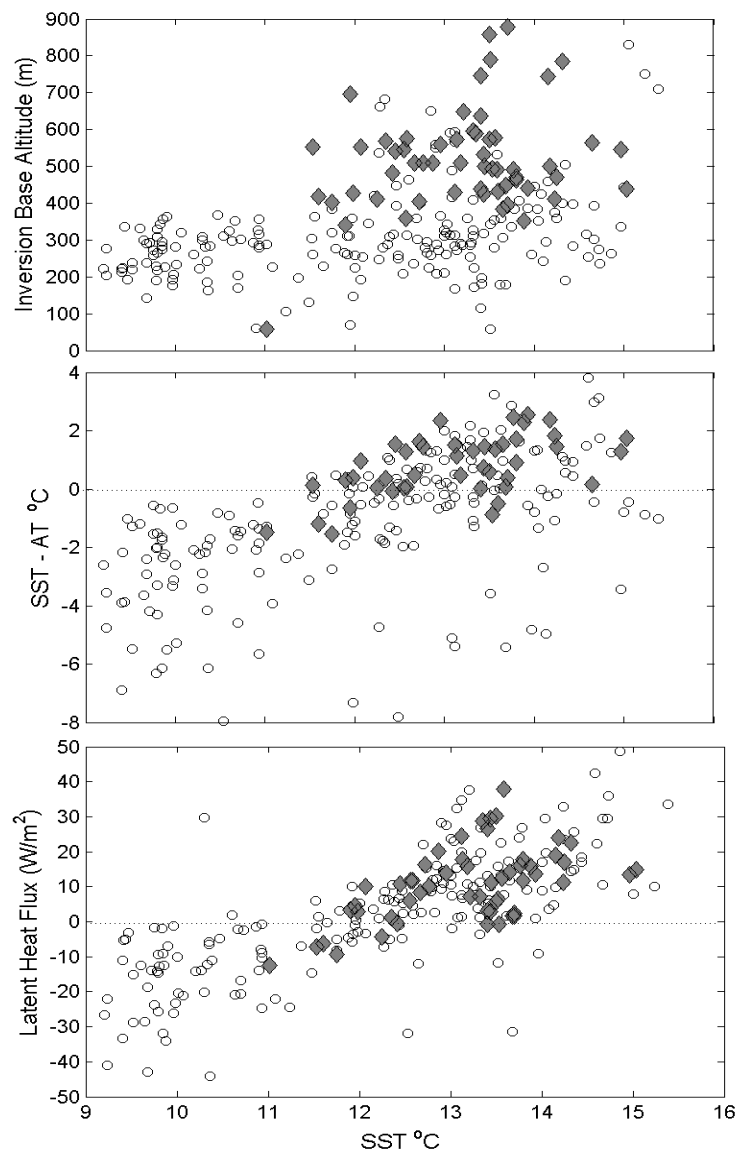


Fig. 5: a) Hourly measured sea surface temperature at NOAA buoy and 6 hourly determinations of the inversion base height from radiosonde temperature measurements (dots). Corresponding times when cloud LWP is  $>100 \text{ g m}^{-2}$  also marked with grey diamonds. b) Differences between buoy measured sea surface temperatures and the radiosonde measured atmospheric temperature at the 0.1 MBL height and the relationship to SST at that time. Times with corresponding LWP measurements greater than  $100 \text{ gm}^{-2}$  marked with (diamonds). c) Buoy measured SST (degrees C) and the calculated, upward latent heat flux ( $\text{W/m}^2$ ). Grey diamonds indicate times when cloud LWP was at least  $100 \text{ g m}^{-2}$ .

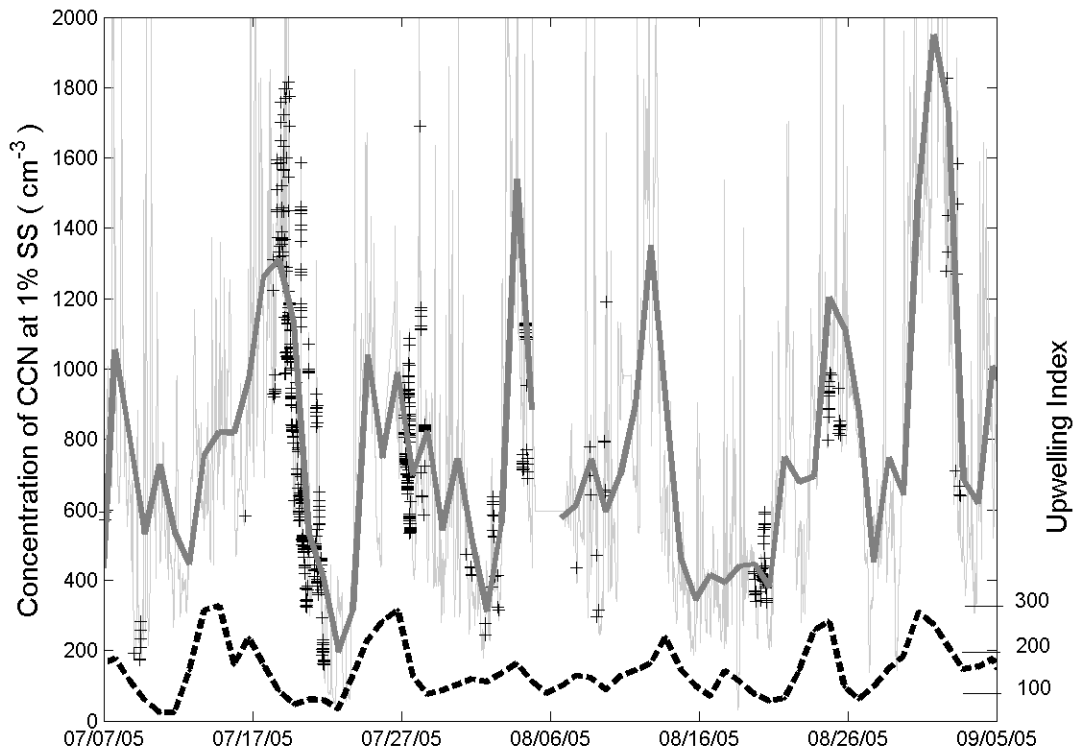


Fig. 6: Daily averaged CCN in  $\text{cm}^{-3}$  at 1% supersaturation (SS) (dark solid) and raw measurements of the same quantity (light solid). Incidents of drizzle are labeled with (+) a cross. The Upwelling Index (dashed line) in units of  $\text{m}^3$  of water per 100 meters of coastline is shown throughout the study time period.

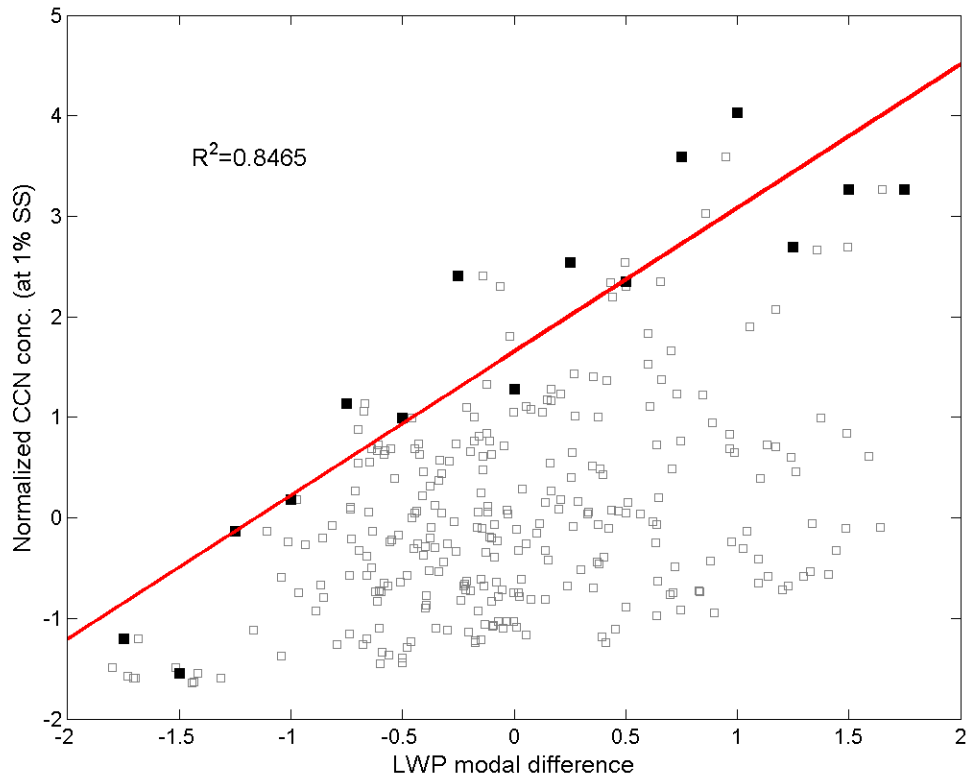


Fig. 7: Open squares: Normalized CCN concentration at 1% supersaturation versus the difference between the observed LWP and the LWP predicted by the first mode of the principal component analysis for all the data collected during nighttime (1am to 5am LST from July 1 to Sept 15, 2005). The data was averaged over 1 minute. Closed squares: Normalized CCN concentration at 1% supersaturation versus the maximum LWP modal difference using 0.25-unit bins for the LWP modal differences. The markers are plotted at the start of each bin. Red Line: Maximum attainable values of the LWP modal difference.

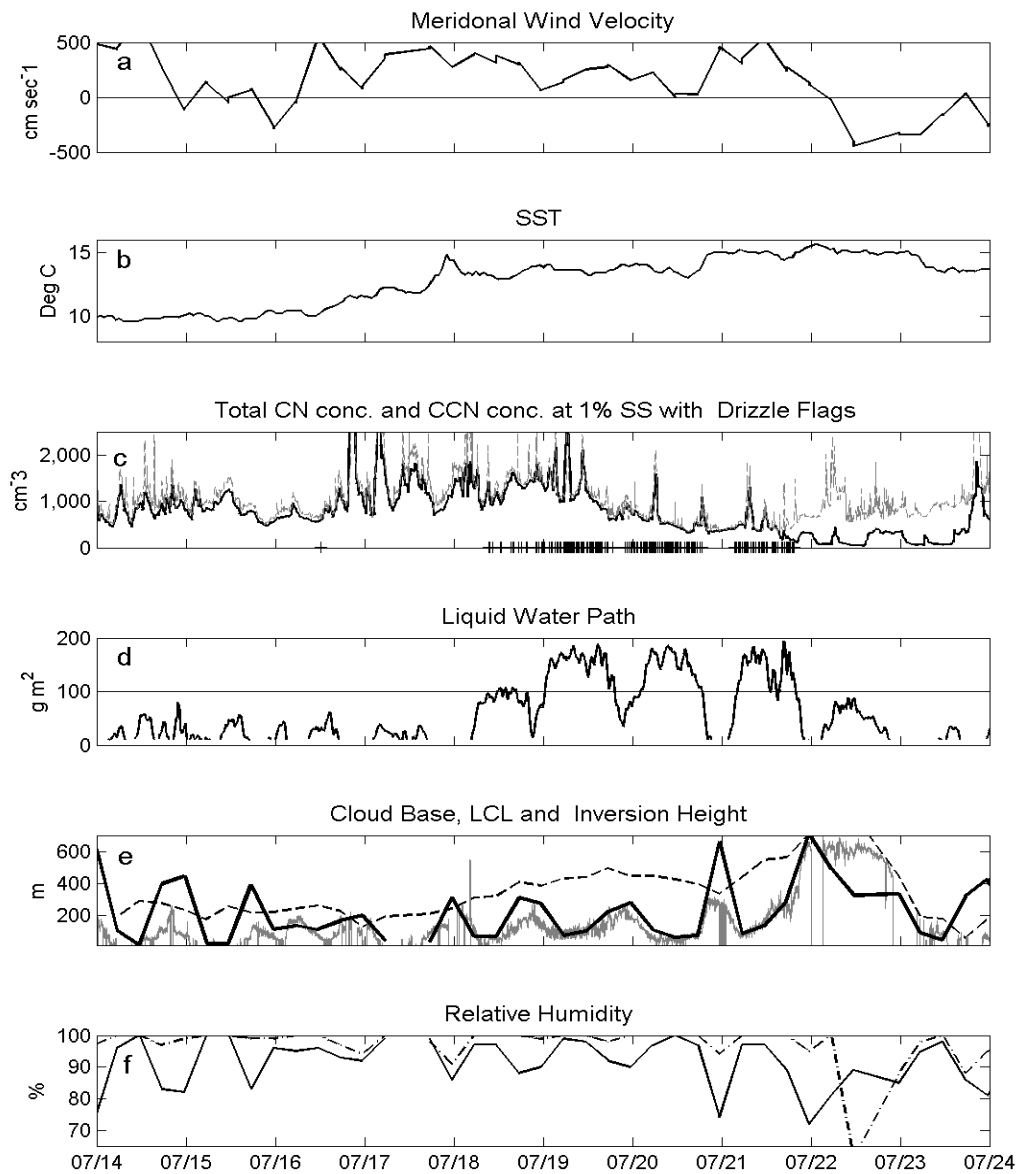


Fig. 8: Conditions observed during Event #3 (a) The meridional component of wind velocity at the AMF site. (b) Offshore Buoy measured SST. (c) The C parameter calculated from CCN spectra collected at the AMF (solid line), total available CN (dotted line) and radar derived drizzle markers (plus sign). (d) Cloud liquid water path measurements collected at the AMF. (e) Ceilometer measured cloud base (solid grey line), inversion height (dashed line) and LCL (dark solid line) as calculated from vertical radiosonde temperature profiles. (f) AMF Radiosonde measured relative humidity at 0.1 (solid line) and 0.9 (dotted line) boundary layer height.

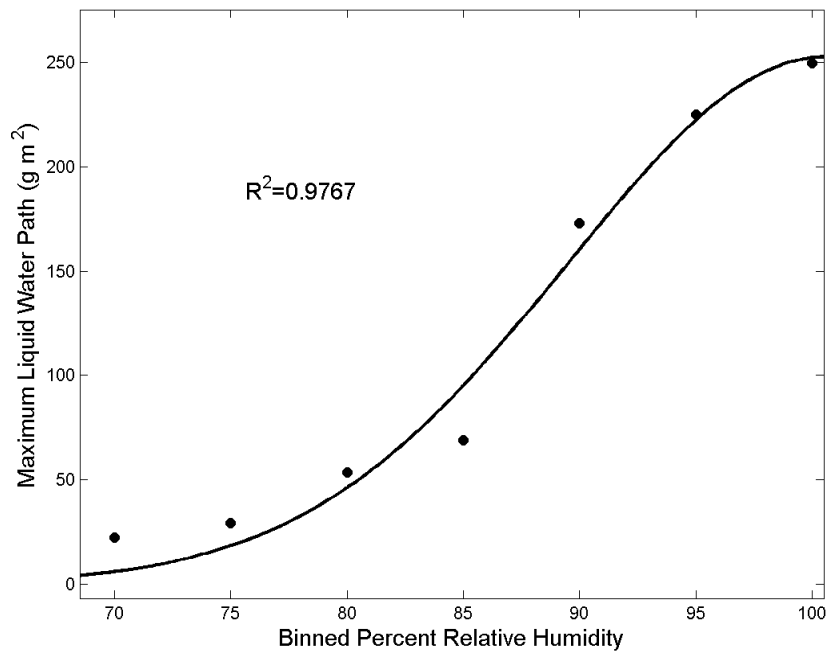


Fig. 9: Six hour averages of nighttime maximum LWP and the radiosonde measured, binned percent relative humidity (5.0 %) determined at the lower (0.1) MBL depth beneath the cloud. Data from July 1 to Sept15, 2005 for 289 total measurements.

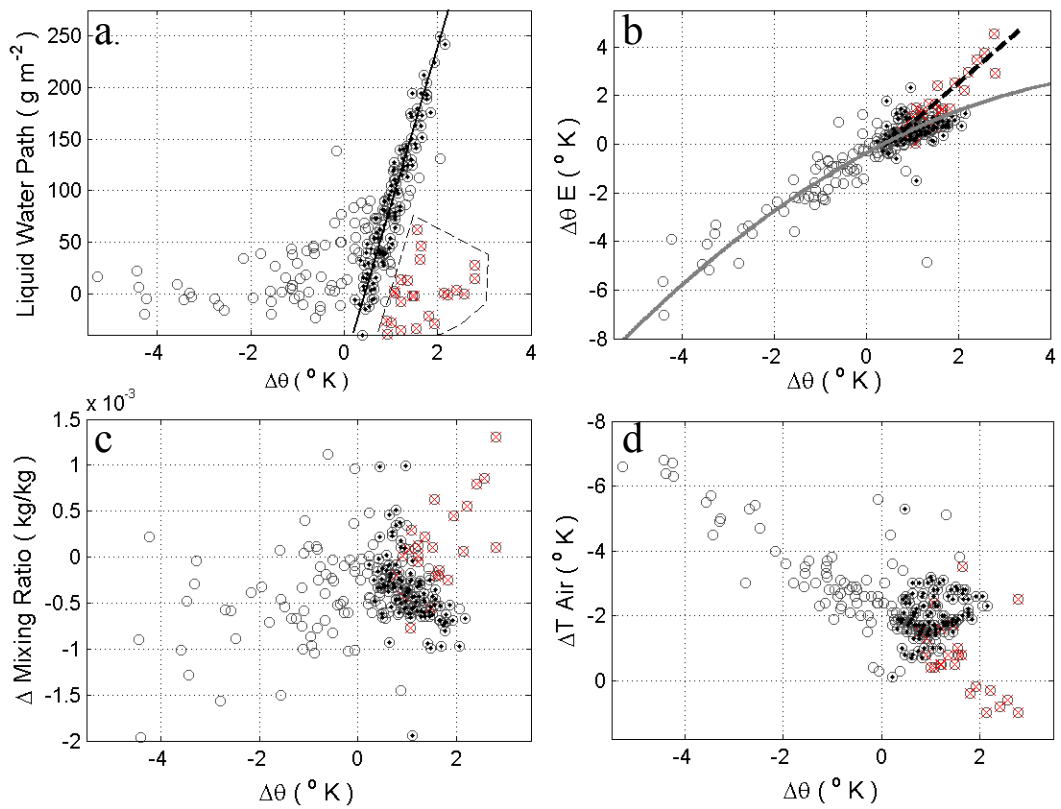


Fig. 10: Vertical differences in potential temperature versus Microphysical and thermodynamic moisture parameters. (a) Liquid water path, (b) equivalent potential temperature, (c) mixing ratio and (d) Vertical environmental temperature difference. Regimes Displayed: 1) open circles: low LWP and low stability, 2) filled circles: Increasing LWP and increasing stability (along solid line), 3) Red X circles: low LWP and high stability.

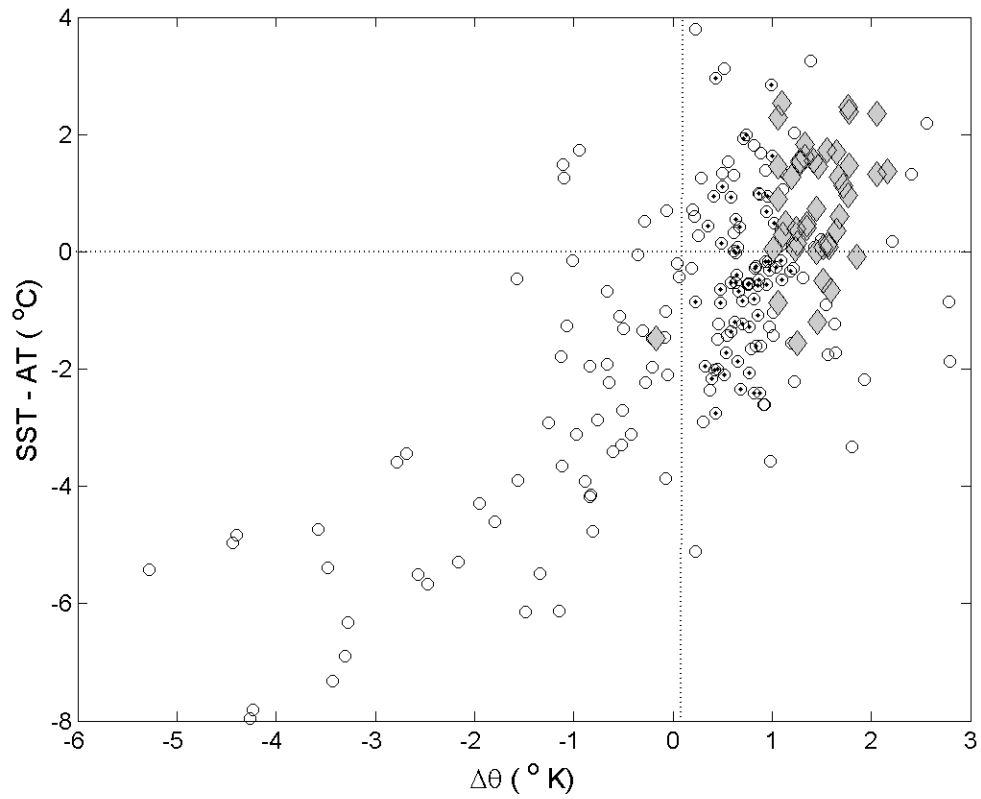


Fig. 11: Differences between buoy measured sea surface temperatures and radiosonde measured atmospheric temperature at the 0.1 MBL height and its relationship with atmospheric stability displayed through vertical difference in potential temperature ( $\Delta\theta$ ) (circles). Times with corresponding LWP measurements greater than  $100 \text{ gm}^{-2}$  marked (diamonds) and stability line points marked (dot).